INSIGHTS INTO THE STRING–BARRIER INTERACTION DYNAMICS BASED ON HIGH-SPEED CAMERA MEASUREMENTS

Dmitri Kartofelev
Tallinn University of Technology,
School of Science,
Department of Cybernetics,
Tallinn, Estonia
dima@ioc.ee

Joann Gustav Arro
Tallinn University of Technology,
School of Science,
Department of Cybernetics,
Tallinn, Estonia
joannarro@gmail.com

Vesa Välimäki
Aalto University,
School of Electrical Engineering,
Department of Signal
Processing and Acoustics,
Espoo, Finland
vesa.valimaki@aalto.fi

ABSTRACT

Analysis of nonlinear phenomena associated with string–barrier collision dynamics is a long-standing open problem in musical acoustics. In order to advance towards a complete understanding of the problem good supporting experimental data are needed. The experimental and theoretical analysis of the string vibration in the monochord equipped with a smooth and rigid barrier is presented. The experimental data are gathered using video-kymographic technique that relies on digital image analysis of high-speed line-scan camera imagery. The data are then compared against a time-stepping model proposed by the authors. The measurements show that the string–barrier dynamics features two distinct vibration regimes. The initial short-lasting *violent* regime characterised by the high energy collisions and the resulting pitch glide effect, and the more *peaceful* regime characterised by the nonlinear inter-modal energy transfer phenomenon. It is shown that the proposed model can predict many aspects of the investigated system. The results and methods presented here should in general find application in string instrument acoustics of similar phenomena.

1. INTRODUCTION

Experimental research into the fundamental mechanical aspects of musical instruments is an important part of the history of musical acoustics and of physics in general. The standard model of a musical instrument has traditionally been based around the canonical picture of a linear resonator, such as an acoustic tube, string, or metal bar, excited by a device with a nonlinear character, such as the lip–reed mechanism, hammer contact, or a friction model of a bow [1]. In recent years, attention has shifted to the nonlinearity in the resonator itself, and the major effect it can have on the resulting sound of the instrument. Two examples are: shock wave propagation in acoustic tubes [2], leading to the brassy timbre of the trombone at high amplitude playing levels; and geometric nonlinearity in thin plate and shell structures, leading to crashes of cymbals [3]. More widespread than either of these two effects is the nonlinearity associated with the collision of a vibrating object such as a string with a barrier. Such an effect plays a dominant role, for example, in guitars and various lutes where the string interacts with a fretboard. It can produce pleasant distortion, increasing the brightness and perceived loudness of the string instrument's sound. However, it has been the most recent nonlinearity to be considered in detail, is least understood, and most lacking in supporting experimental data.

The theoretical study and modeling of string–barrier interaction are long-standing open problems in musical acoustics. In the early twentieth century, Raman [4] was first to study the problem and identify the veena bridge as the main reason for the distinctive sound of the tambura and veena. He noted that all string frequencies in these instruments are excited irrespective of the location of the excitation thereby violating the Young-Helmholtz law which states that the vibrations of a string do not contain the natural modes which have a node at the point of excitation. He notes that this is caused by the geometry of the bridge but did not explain the reason behind the inapplicability of the Young-Helmholtz law. Since then, much effort has been devoted to modeling the collision dynamics of a vibrating string with various obstacles or boundary barriers. Over the years many authors have solved this problem using different approaches: method of characteristics [5, 6]; assuming an inelastic constraint where the string is losing kinetic energy during contact [7]; physical modeling accompanied by the finite difference method [8–14]; a modal analysis approach [15–17]; by describing the movement of the sitar string with partial differential equations [18–20]; waveguide modeling [21–23]; and finite element method with Ivanov transformation to integrate the problem [24].

Some direct experimental measurements of string vibration in various string–barrier systems have been previously conducted. The methods of string displacement measurement can be divided into three categories: electromagnetic methods, electric field sensing, and optical methods. The electromagnetic methods exploit Faraday's law. The principle of the string displacement detection is the following: An electromagnetic coil is placed near the string, and the motion of the string induces a voltage in the circuit that

Copyright: © 2020 Dmitri Kartofelev et al. This is an open-access article distributed under the terms of the Creative Commons Attribution 3.0 Unported License, which permits unrestricted use, distribution, and reproduction in any medium, provided the original author and source are credited.

is proportional to the string's velocity from which the displacement of the string is obtained. This method was used and described in [25, 26]. The electric field sensing method makes use of the phenomenon of capacitance change between two electrodes, when the distance between them is varied. In the simplest approach, a conducting string is grounded, and direct current (DC) is applied to an electrode plate. The string's movement modulates the voltage between the string and the plate, and thus information about the string's displacement is obtained (*cf.* [27]). The optical methods exploit various light or laser emitting and detecting sensors to capture vibration. For example, high-speed cameras with suitable video analysis have been used to measure string vibration successfully [28]. Also, different devices that convert laser rays into a uniform parallel beam and detect their shadows can ensure the result [29]. Devices that are based on various photovoltaic detectors have also been successful [30].

Our experimental approach can be classified under the aforementioned optical methods. The non-invasive video-kymographic method based on the exploitation of digital high-speed line-scan camera (LSC) is used. The method has been used successfully in musical acoustics research [31–34].

In this paper a monochord equipped with a rigid barrier with circular cross-section profile made from rigid polyvinyl chloride plastic is experimentally investigated. This type of plastic has compression strength $\approx$ 66 MPa which is comparable to concrete. Figure 1a shows the position of the barrier with respect to the speaking length of the string. The experimentally obtained string vibration data are then compared against a simplified theoretical model, proposed by the authors, with the aim to deduce some beneficial conclusions in addition to the direct observations. The model assumes frequency-independent lossy *ideal* string vibration. The interaction between the vibrating string and the barrier is modeled in terms of kinematics, i.e., we study the string motion without considering its mass nor the possible inertial and reactional forces acting between the string and the barrier while colliding. The heuristics of our approach are directly determined by d'Alembert formula (traveling wave solution). Modeling approach presented here is a continuation of the work done in [34–36].

The organisation of the paper is as follows: Secs. 2 and 3 present the numerical time-stepping model of string–barrier interaction; in Sec. 4, the experimental approach and setup are further clarified; Sec. 5 compares the experimental results with the model output and presents our findings; Sec. 6 presents the conclusions.

2. STRING VIBRATION MODEL

We consider vibration of a lossy ideal string in a single vibration plane described by one-dimensional wave equation

$$\frac{\partial^2 u}{\partial t^2} = c^2 \frac{\partial^2 u}{\partial x^2} - 2\alpha \frac{\partial u}{\partial t}, \tag{1}$$

where $u(x,t)$ is the transverse displacement of the string, $c = \sqrt{T/\mu}$ is the speed of the waves traveling on the string, T is the tension and μ is the linear mass density (mass

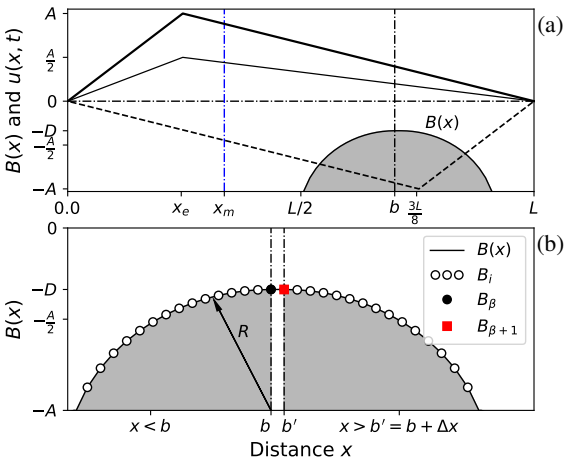

Figure 1. (a) Schematic of the problem studied. Triangular initial condition $u(x,0)$ exited at $x = x_e = L/4$ is shown with the solid black line, and corresponding (overlapped) traveling waves $r(x,0)$ and $l(x,0)$ are shown with the thin line. The barrier is shown with the grey formation located at $x = b$. The resting position of the string is shown with the horizontal dash-dotted line. String position in the absence of the barrier $u(x, P/2)$ after half a period P is shown with the dashed line. LSC measurement point $x = x_m$ is shown with the blue dash-dotted line. (b) Cross-section profile $B(x)$ of the barrier and its discrete samples B_i, where $B_\beta = B_{\beta+1} = -D$.

per unit length) of the string. In the context of a real string Eq. (1) can be used as a valid approximation of *thin* homogeneous elastic string vibration under a *small* amplitude restriction. In this case wave speed $c = \sqrt{T/\mu} = \sqrt{T/\rho A}$, where ρ is the volumetric density of string material (nylon) and A is the cross-section area of a cylindrical string. The second term on the right-hand side of Eq. (1) introduces frequency-independent loss. It is easy to show that for $\alpha > 0$ all frequency components will decay $\sim e^{-\alpha t}$. This term can be seen as a perturbation term acting on the wave equation in the form

$$\frac{\partial^2 u}{\partial t^2} = c^2 \frac{\partial^2 u}{\partial x^2}, \tag{2}$$

thus its linear effects on the final solution can be added separately. For now we focus on Eq. (2). It is well known that Eq. (2) has an analytical solution—d'Alembert formula. For an infinite string (ignoring boundary conditions for now), for initial conditions $u(x,0) = u_0(x)$, and $\partial u(x,0)/\partial t = 0$ the solution takes the following form:

$$u(x,t) = \left(u_0(x - ct) + u_0(x + ct)\right)/2. \tag{3}$$

This solution represents the superposition of two traveling waves: $u_0(x - ct)/2$ moving to the right (positive direction of the x-axis); and $u_0(x + ct)/2$ moving to the left. Function $u_0/2$ describes the shape of these waves and stays constant with respect to x-axis, as they are translated in opposite directions at speed c [37].

In general, a wave on any arbitrary segment of the string can be understood as a sum of two traveling waves that do not need to be equal. It can be written

$$u(x,t) = r(x-ct) + l(x+ct), \tag{4}$$

where $r(x-ct)$ is the traveling wave moving to the right and $l(x+ct)$ is the traveling wave moving to the left.

A well-known time-stepping method for implementing d'Alembert formula is the following. We discretise xt-plane into $n \times m$ discrete samples. We discretise the x-axis with grid spacing $\Delta x = L/n$ where L is the speaking length of the string, and the t-axis with grid spacing $\Delta t = t_{\text{max}}/m$, where t_{max} is the integration time. We let $x_i = i\Delta x$, where $0 \le i \le n$ and $t^j = j\Delta t$, where $0 \le j \le m$. Additionally, the values of Δx, Δt, n and m are selected such that

$$\frac{c}{2L} = \frac{\Delta x/\Delta y}{2L} = \frac{\sqrt{T/\mu}}{2L} = \frac{\sqrt{T/\rho A}}{2L} = f_0, \tag{5}$$

where f_0 is the fundamental frequency of the string [37, 38]. From here it follows that $u_i^j = u(x_i, t^j)$, $r_i^j = r(x_i, t^j)$, and $l_i^j = l(x_i, t^j)$. And, by applying

$$r_i^{j+1} = r_{i-1}^j \quad \text{and} \quad l_i^{j+1} = l_{i+1}^j, \tag{6}$$

for all grid points i and j in a sorted order one gets the translation of numerical values r_i^j and l_i^j propagating in opposite directions with respect to x_i-axis. This result agrees with d'Alembert formula (3) or (4) and can be understood as a digital waveguide based on traveling wave decomposition and use of two delay lines. The equivalence between the model used here and the digital waveguide modeling is shown in [37, 38].

So far we have not addressed the boundary conditions of Eq. (2). We assume that the string is fixed at both ends. The following boundary conditions apply:

$$u(0,t) = u(L,t) = 0, \quad t \in [0, t_{\text{max}}], \tag{7}$$

where $t_{\text{max}} > 0$ is the desired integration time. By applying boundary conditions (7) to general solution (4) the reflected traveling wave located at $x = 0$ can be found in the following form:

$$u(0,t) = r(-ct) + l(ct) = 0 \Rightarrow r(-ct) = -l(ct), \tag{8}$$

and similarly for $x = L$:

$$u(L,t) = r(L-ct) + l(L+ct) = 0 \Rightarrow \\ \Rightarrow l(L+ct) = -r(L-ct). \tag{9}$$

These results are discretised according to the discretisation scheme discussed above. The traveling wave (8) reflected from the left boundary at $x = 0$ takes the form

$$r_0^j = -l_0^j, \quad j \in [0, m], \tag{10}$$

and the traveling wave (9) reflected from the right boundary at $x = L$ takes the form

$$l_n^j = -r_n^j, \quad j \in [0, m]. \tag{11}$$

In order to obtain the resulting string displacement u_i^j, for the selected initial and boundary conditions, a superposition of traveling waves (6), (10), and (11) is found in accordance with general solution (4)

$$u_i^j = r_i^j + l_i^j, \quad i \in [0, n],\ j \in [0, m]. \tag{12}$$

Finally, there remains only the question of loss introduced in Eq. (1). Since loss is $\sim e^{-\alpha t}$ in the continuous domain and $\sim e^{-\alpha j \Delta t}$ in the discrete domain then the loss factor per single time step Δt is

$$\frac{e^{-\alpha(j+1)\Delta t}}{e^{-\alpha j \Delta t}} = e^{-\alpha \Delta t (j+1-j)} = e^{-\alpha \Delta t}. \tag{13}$$

We introduce loss by updating (6) to

$$r_i^{j+1} = r_{i-1}^j e^{-\alpha \Delta t} \quad \text{and} \quad l_i^{j+1} = l_{i+1}^j e^{-\alpha \Delta t}. \tag{14}$$

3. STRING–BARRIER INTERACTION MODEL

We consider a smooth and absolutely rigid impenetrable obstacle. The obstacle is placed near the vibrating string so that it is able to obscure string displacement $u(x,t)$, see Fig. 1a. For simplicity, we select a barrier with circular cross-section profile

$$B(x) = -R - D + \sqrt{R^2 - (x-b)^2}, \tag{15}$$

where $x = b$ is the position of the barrier along the string, D is the vertical proximity of the barrier to the string at its rest position, and R is the radius of the positive half circle. The function $B(x)$ is discretised according to the discretisation scheme presented in Sec. 2. We let $B_i = B(x_i)$. Figure 1 shows cross-section profile function $B(x)$ and its discretised samples B_i in addition to the barrier position with respect to the string.

The kinematic modeling of the string–barrier interaction is a twofold problem. First, traveling wave $r(x-ct)$ approaching the barrier form the left side is considered. Secondly, traveling wave $l(x+ct)$ approaching the barrier from the right side is considered.

3.1 Reflection of traveling wave $r(x-ct)$

The heuristics of the following approach are strictly determined by d'Alembert formula (3) or (4). Any change in string displacement $u(x,t)$ imposed by the barrier must involve both traveling waves that compose it. The reflection of traveling wave $r(x-ct)$ approaching the barrier from the left is determined by a change in traveling wave $l(x+ct)$. We assume that the traveling wave $l(x+ct)$ resulting from the interaction first appears, or already existing one is modified, only at the point $x = x^* \le b$, where the amplitude of string displacement $u(x^*,t) < B(x^*)$. The position of this point x^* is determined by barrier profile geometry $B(x)$. Since, the barrier is impenetrable we must have $u(x^*,t) = B(x^*)$ during the collision. This condition determines the shape of the *reflected* traveling wave

$$\hat{l}(x^*,t) = B(x^*) - u(x^*,t). \tag{16}$$

After determining the shape of the *reflected* traveling wave given by (16) it is used to modify the existing traveling wave $l(x+ct)$ in the following manner:

$$l(x^*,t) = l(x^*,t) + \hat{l}(x^*,t). \tag{17}$$

The above modification of traveling wave $l(x+ct)$ simply ensures that the resulting string displacement $u(x^*,t) = r(x^*,t) + l(x^*,t)$ does not penetrate the barrier $B(x)$.

The determination of points x^* do not require consideration of points $x > b$. In the absence of any waves approaching from the right and for $x^* = b$ the string displacement $u(b,t) = -D$ (caused by the reflection process explained in Sec. 3.2). This means that the string displacement $u(x,t)$ becomes truncated and equal to the maximum value of the circular barrier as the propagating wave passes over its apex. This phenomenon is shown in Fig. 2 in the case of a short wavelength (width) inverted bell-shaped pulse reflecting from the barrier during the first period of vibration. Because, the barrier profile is a half-circle with its maximum at $x = b$, then for $x > b$ it holds that $u(x,t) > B(x) \Rightarrow x \neq x^*$.

The numerical implementation of this procedure is straightforward. We let $x_\beta = \beta\Delta x = b$ (see Fig. 1) and $x_{i^*} = i^*\Delta x = x^*$. Using this notation the *reflected* traveling wave (16) takes the following form:

$$\hat{l}^j_{i^*} = B_{i^*} - u^j_{i^*}, \quad i \in [0,\beta]. \tag{18}$$

The resulting reflection and consequent string shape according to (12) and (17) for grid points i^* takes the form

$$u^j_{i^*} = r^j_{i^*} + l^j_{i^*}, \quad i \in [0,\beta], \tag{19}$$

where

$$l^j_{i^*} = l^j_{i^*} + \hat{l}^j_{i^*}, \quad i \in [0,\beta]. \tag{20}$$

3.2 Reflection of traveling wave $l(x+ct)$

The determination of the reflection of traveling wave $l(x+ct)$ approaching the barrier from the right side is similar to the previous case. In fact, it is a mirror image of that problem with the symmetry axis at $x = b$. However, there is a slight difference in the region where it is necessary to evaluate and determine points $x = x^*$. This difference stems from the selection of barrier cross-section profile (15), namely, function $B(x)$. Since, $B(x)$ is a smooth unimodal (single *humped*) function, it has one maximum $\max B(x) = -D$ at $x = b$. The problem arises from the fact that one has already evaluated this point inside the same time moment t, and used it to calculate the reflection of traveling wave $r(x-ct)$. By using this point again one would introduce an undesired discontinuity in the string displacement $u(x,t)$. In principle it is not possible to use some other closely located neighbouring point, e.g., $x = b' = b + \Delta x$ (see Fig. 1). This selection, too, would introduce a small discontinuity due to $B(b) \neq B(b')$, and more importantly, in the continuous domain of real numbers there is no such thing as the neighbouring number because the set of real numbers is uncountable. One way of resolving this problem is to slightly modify the discretised

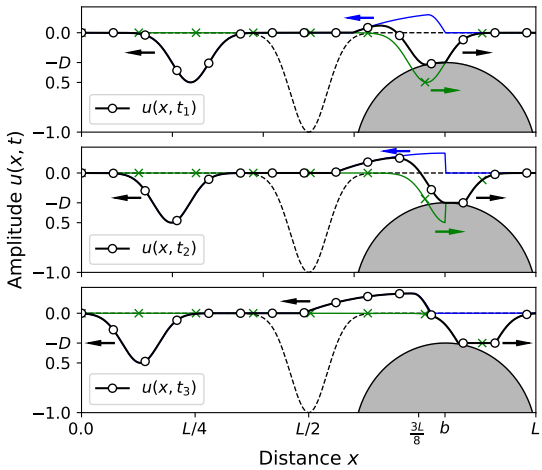

Figure 2. Reflection of traveling wave $r(x-ct)$, shown with the thin marked green line, from the barrier that is shown with the grey formation. Reflected traveling wave $\hat{l}(x+ct)$ is shown with the thin blue line. Resulting string shape $u(x,t)$ is shown with the bold marked line. Arrows indicate the directions of wave propagation. Bell-shaped initial condition is shown with the dashed line. Results are shown for three time moments, such that $t_1 < t_2 < t_3$.

approximation of barrier profile B_i as shown in Fig. 1b. A second maximum point $B_{\beta+1} = -D$ is simply squeezed in after the grid point $i = \beta$ corresponding to $x_\beta = \beta\Delta x = b$. Because $\Delta x \ll 1$ the overall change introduced in B_i compared to $B(x)$ remains negligibly small.

This problem arises only for symmetric unimodal functions $B(x)$ with their symmetry axis passing through a discrete grid point i. Alternatively to the solution proposed above, one could also redefine $B(x)$ so that two neighbouring grid samples i, e.g., β and $\beta+1$ would straddle the symmetry peak, i.e., the peak would occur at the midpoint between two samples. It must be noted that for barriers with monotonic flat peaks this problem can be ignored.

Let us formalise the final result. Similarly to the previous case only at the points $x = x^* \geq b'$ a reflected traveling wave moving to the right is introduced in the following form:

$$r(x^*,t) = r(x^*,t) + \hat{r}(x^*,t), \tag{21}$$

where

$$\hat{r}(x^*,t) = B(x^*) - u(x^*,t). \tag{22}$$

The numerical implementation, using the notation proposed in Sec. 3.1, is the following: the resulting reflection and consequent string shape according to (12), (21), and (22) for grid points i^* takes the form

$$u^j_{i^*} = r^j_{i^*} + l^j_{i^*}, \quad i \in (\beta,n], \tag{23}$$

where

$$r^j_{i^*} = r^j_{i^*} + \hat{r}^j_{i^*} \text{ and } \hat{r}^j_{i^*} = B_{i^*} - u^j_{i^*}, \text{ if } i \in (\beta,n]. \tag{24}$$

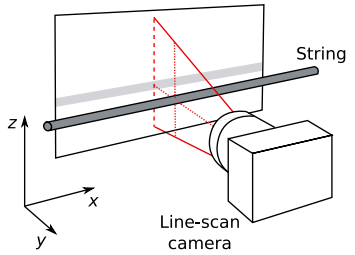

Figure 3. Placement of the LSC with respect to the vibrating string. Geometry of the area that is being imaged (the *line*) is shown with the vertical dotted red line. Transverse string vibration takes place in the xz-plane.

4. EXPERIMENTAL SET-UP

The transverse uniplanar displacement of a single point along the string is measured using the high-speed LSC. The camera produces two-dimensional images (not videos) called the *kymographs*. The geometry of the digital imaging sensor of the LSC differs from sensors found in commonly used video cameras. Usually, the video camera sensor pixels are placed in rows and columns forming a grid. The LSC sensor consists only of a single pixel array, referred here to, as the *line*, see Fig. 3. While filming the camera continuously stacks these *lines* to form an image. Figure 3 also shows the placement of the LSC with respect to the string while recording.

The transverse string displacement time-series extraction is based on the discrete one-dimensional convolution integral of the individual kymograph lines

$$s[i] = (p * k)[i] = \sum_{n=-\infty}^{\infty} p[n]\, k[i-n], \qquad (25)$$

where $i \in [1, 1024]$ is the pixel number in any given *line*, $p[i]$ is the image depth value in bits, $k[i]$ is the convolution kernel. Kernel $k[i]$ is selected to be similar in shape to the string (its *line*/image), this guarantees that convolved *line* $s[i]$ has a clear and unique maximum that will coincide with the string position with respect to the measured *line*. Thus, for any given *line*, pixel i corresponding to string position

$$i = \arg(\max s[i]). \qquad (26)$$

This procedure is repeated for all *kymograph lines*. The additional explanation and examples of applying formula (25) can be found in [31, 32]. Figure 4a shows an example of *kymograph* recording and the result of the aforementioned image analysis. Figure 4b shows the calibrated time-series where the *line* number is multiplied by $dt = 1/44100$ s since the camera is recording at audio sampling rate of 44100 lines/s, and the *line* pixel number is multiplied by dx which value is determined by filming a high-contrast calibration sheet with known dimensions. The accurate calibration is of paramount importance because the string–barrier system features a strong amplitude nonlinearity.

In this study we use the controlled and repeatable string excitation method explained in [34]. The string point

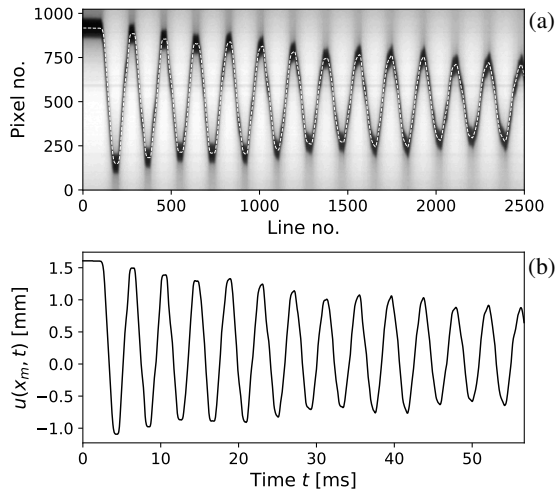

Figure 4. (a) Kymograph of transverse string displacement $u(x_m, t)$. String displacement tracking with line convolution method (25) is shown with the overlaid dashed line. (b) Calibrated string displacement time-series $u(x_m, t)$ corresponding to the kymograph above.

$x = x_e$ is displaced to a desired amplitude with the aid of a cotton thread and abruptly released by burning the thread. This method of string excitation produces triangular shaped initial condition shown in Fig. 1a and guarantees uniplanar vibration of the string [34]. Figure 1a also shows the position of measurement point x_m, excitation point x_e (tip of the triangle), and the placement of the barrier along the string's speaking length $x \in [0, L]$.

The following parameter values of the experimental set-up shown in Fig. 1 are used: speaking length of the unwound nylon guitar string[1] $L = 0.66$ m; fundamental frequency $f_0 = 196$ Hz (if not stated otherwise); excitation point $x = x_e = L/4 = 0.165$ m; initial amplitude $A = 1.85$ mm; barrier position $x = b = 0.735L = 0.485$ m; barrier's proximity to the string at its rest position $D = 1.61$ mm; barrier radius $R = 0.1$ m; loss parameter $\alpha = 9$ s^{-1}. All time and frequency-domain result are shown or calculated for string displacement $u(x_m, t)$ where measurement point $x_m = 0.41L = 0.235$ m. The spectrograms of power spectra, amplitude spectra and instantaneous spectral centroid $\langle f' \rangle(t)$ are calculated using the Fast Fourier Transform algorithm. In calculating spectrograms a sliding window approach, in combination with Hanning window function are used. Here, window size is 45 ms and window overlap value is 80%. Instantaneous spectral centroid $\langle f' \rangle(t)$ is calculated with the window size 40 periods and overlap of 16 periods, precisely. The (example) numerical parameters of the model presented in Secs. 2 and 3 are the following: $n = 1105$, $\Delta x \approx 6.0 \cdot 10^{-4}$ m, $m = 68\,796$, $\Delta t \approx 1.9 \cdot 10^{-6}$ s (resulting in 130 ms of vibration, shown in Fig. 5).

[1] String set: Earthwood Light 2148. String gauge: 15. Manufacturer: Ernie Ball Inc. Coachella, California, USA 92236

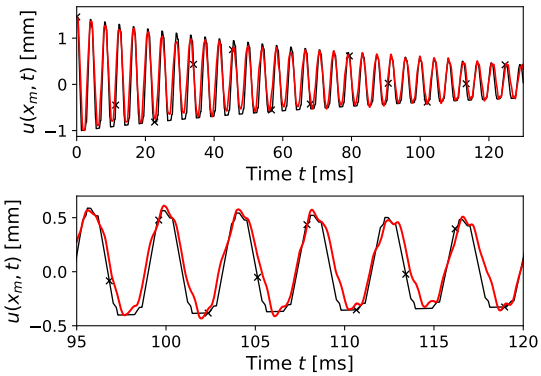

Figure 5. Transverse vibration of the string $u(x_m, t)$. Comparison of a typical experimental result shown with the red line and the model shown with the marked line. Here, the model is tuned to $f_0 = 240$ Hz—the initial pitch glided frequency valid for $t \lesssim 0.25$ s.

5. RESULTS AND DISCUSSION

Analysis of repeated experiments shows that the resulting string–barrier dynamics can be divided into two distinct regimes. The initial short-lasting *violent* regime dominated by the high amplitude collisions and the resulting pitch glide effect, and the more *peaceful* regime dominated by the nonlinear energy transfer phenomena. The frequency-domain results shown/discussed below indicate that the temporal dividing line between these regimes $t \approx 0.25$ s.

Figure 5 compares the model output to a typical experimental measurement for the first 130 ms of vibration. The shapes of waveforms $u(x_m, t)$ match up relatively well, given the simplicity of our model and the nonlinearity of the experiment. During the experiments it was discovered that the monochord tuned to $f_0 = 196$ Hz vibrated at frequency 240 Hz for $t \lesssim 0.25$ s (*violent* regime). This frequency lies almost precisely between 196 Hz the frequency related to speaking length $L = 0.66$ m and 278 Hz the frequency related to speaking length $b = 0.485$ m. Eventually, for $t \gtrsim 0.25$ s (*peaceful* regime), the frequency settles down to the nominal frequency of 196 Hz. Although, our model is capable of generating pitch glided outcomes (e.g., for smaller D) [39] the glide is not accurately reproduced for the actual parameters used in the experiment. The glide in the modelled data is much smaller than in the experiment. Hence, the *incorrect* tuning of the model in Fig. 5. The most likely explanation for this discrepancy is the fact that our model ignores the stiffness of the real string.

The time-domain explanation of the pitch glide is the following: The pitch is higher at the beginning of the vibration, because of the *effective* shortening of the speaking length L due to the spatial extent of the barrier and the string–barrier interaction. The segment of the string that "clings" to the barrier, as it collides with it, is temporarily forced not to participate in the vibration. This makes the actively moving part of the string slightly shorter for a fraction of the period and thus raising the average value of the fundamental frequency. This phenomenon also explains the fact that a stiff string must feature more prominent pitch glide. The stopped string segment is shorter in the case of ideal string that is capable of wrapping itself around the barrier whereas it is much harder to wrap a stiff string around it. This means that the *effective* shortening of the speaking length L is greater in the case of a stiff string—the experiment.

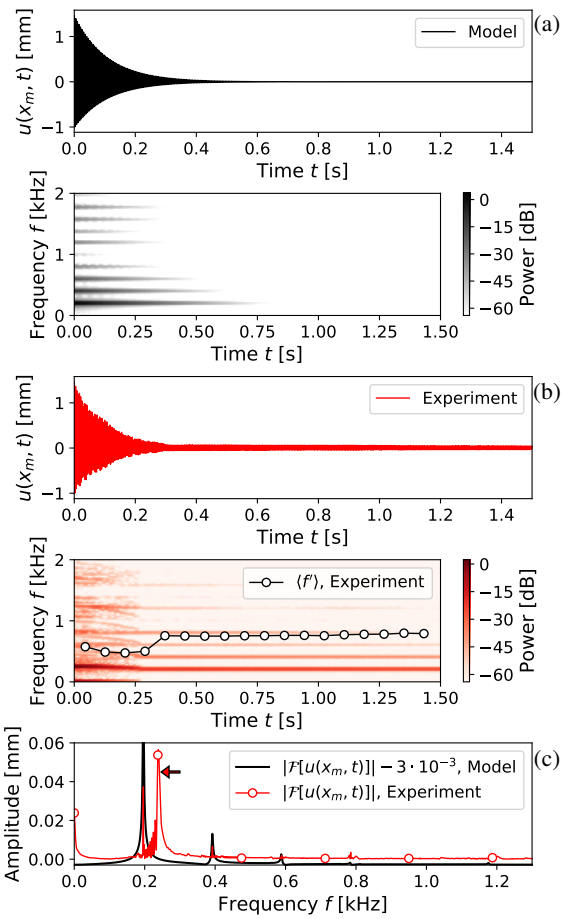

Figure 6. Spectral analysis of the model (a) and the experiment (b). Instantaneous spectral centroid $\langle f' \rangle(t)$ is shown with the marked line. (c) Amplitude spectra of the above time-domain signals. Spectral peak indicated by the arrow corresponds to frequency 240 Hz.

Figure 6 shows the frequency-domain results for the *correctly* tuned model, where $f_0 = 196$ Hz. The initial pitch glide is clearly visible on the spectrogram of the typical experiment. The glide is also confirmed by the spectral centroid $\langle f' \rangle(t)$ graph for $t \lesssim 0.25$ s. For $t \approx 0.3$ s centroid shifts abruptly upwards, which is explained by the diminished average amplitude (less *violent* collisions) and the nonlinearity of the problem. The string–barrier collisions force energy to move from the lower partials to the higher ones. The visual inspection of the centroid $\langle f' \rangle(t)$ graph shows that after the abrupt change at $t \approx 0.3$ s the centroid continues to slowly creep upwards towards higher frequencies as predicted by nonlinear theories. The comparison of

the model and experimental spectrograms suggests that our model is not suitable for sound synthesis applications.

The amplitude spectrum, shown in Fig. 6c reveals that a 0 Hz DC component is present. Most likely, it is also related to the pitch glide phenomenon. More precisely, to the most *violent* initial stages of the vibration, when the barrier is heavily restricting the string displacement by forcing it to a stop. Again, although the duration of this *stopping* lasts for only a fraction of period it is, nevertheless, picked up by the Fourier transform. The amplitude spectrum in Fig. 6c shows a clear peak corresponding to the initial higher pitch $f = 240$ Hz present for $t \lesssim 0.25$ s discussed above. This peak is missing from the modeled result.

6. CONCLUSIONS

The experimental measurements conducted for this paper revealed that the string–barrier dynamics features two distinct vibration regimes. The initial short-lasting *violent* regime characterised by the high energy collisions and the resulting pitch glide effect, and the more *peaceful* regime characterised by the nonlinear inter-modal energy transfer.

The method of modeling string–obstacle interaction presented in this paper is probably one of the most simplified and idealised approaches that is still able to retain scientific relevance and provide a useful insight into more realistic problems. This was proven by its ability to predict the string displacement, as shown in Fig. 5, quite accurately. The idealised nature of the method guarantees numerical robustness. The biggest mismatch between our model and the experiment was the magnitude of the pitch glide phenomenon, which for the actual experimental parameters, was not sufficiently reproduced by our model. The most likely explanation for this discrepancy is the fact that our model ignores string stiffness. The proposed approach can be applied for estimating the effect that an obstacle with various cross-section profiles has on a string vibration—a beneficial tool in musical acoustics research. Additionally, the model can be used to study the effects of different initial and plucking conditions, including dynamic ones, on a string–barrier system dynamics. Using the tools of signal processing and sound synthesis the presented model can be improved so to synthesise sounds of string instruments that are equipped with nonlinearity inducing obstacles, such as, frets, bridges, snares and nuts.

The video-kymographic experimental measurement technique used in this paper has proven to be highly reliable for our purposes. The method was able to measure submillimetre objects and displacements. Therefore it is suitable in applications where high spatial and temporal resolutions of measurements are required.

Acknowledgments

This work is part of the activities of the Nordic Sound and Music Computing Network—NordicSMC, NordForsk project number 86892. D. Kartofelev and J. Arro were supported by Estonian Min. of Edu. and Res. (IUT33-24) and Doctoral Studies and Internationalisation Prog. DoRa Plus (Archimedes Found., Estonia). The authors are grateful to the Aalto Uni. funding scheme for infrastructure. The measurements for this study were made in Dec. 2018, when D. Kartofelev and J. Arro visited the Aalto Acoustics Lab.

7. REFERENCES

[1] N. H. Fletcher and T. D. Rossing, *The Physics of Musical Instruments*. USA: Springer, 1998.

[2] A. Hirschberg, J. Gilbert, R. Msallam, and A. P. J. Wijnands, "Shock waves in trombones," *J. Acoust. Soc. Am.*, vol. 99, no. 3, pp. 1754–1758, 1996.

[3] C. Touzé, O. Thomas, and A. Chaigne, "Asymmetric non-linear forced vibrations of free-edge circular plates. Part 1: Theory," *J. Sound Vib.*, vol. 258, no. 4, pp. 649–676, 2002.

[4] C. V. Raman, "On some Indian stringed instruments," *Proc. Indian Assoc. for the Cultivation of Sci.*, vol. 7, pp. 29–33, 1921.

[5] M. Schatzman, "A hyperbolic problem of second order unilateral constraints: the vibrating string with a concave obstacle," *J. Math. Anal. and Appl.*, vol. 73, no. 1, pp. 138–191, 1980.

[6] H. Cabannes, "Presentation of software for movies of vibrating strings with obstacles," *Appl. Math. Lett.*, vol. 10, no. 5, pp. 79–84, 1997.

[7] R. Burridge, J. Kappraff, and C. Morshedi, "The sitar string, a vibrating string with a one-sided inelastic constraint," *SIAM J. Appl. Math.*, vol. 42, no. 6, pp. 1231–1251, 1982.

[8] M. Ducceschi, S. Bilbao, and C. Desvages, "Modelling collisions of nonlinear strings against rigid barriers: Conservative finite difference schemes with application to sound synthesis," in *Proc. 22nd Int. Cong. on Acoust.*, Buenos Aires, Argentina, Sept. 5–9 2016, pp. 1–11.

[9] A. Krishnaswamy and J. O. Smith, "Methods for simulating string collisions with rigid spatial obstacles," in *Proc. IEEE Workshop on Appl. of Sig. Proc. to Audio and Acoust.*, New Paltz, NY, USA, 2003, pp. 233–236.

[10] S. M. Han and M. A. Grosenbaugh, "Non-linear free vibration of a cable against a straight obstacle," *J. Sound Vib.*, vol. 237, pp. 337–361, 2004.

[11] S. Bilbao, A. Torin, and V. Chatziioannou, "Numerical modeling of collisions in musical instruments," *Acta Acust. united Ac.*, vol. 101, no. 1, pp. 155–173, 2012.

[12] V. Chatziioannoua and M. van Walstijn, "Energy conserving schemes for the simulation of musical instrument contact dynamics," *J. Sound Vib.*, vol. 339, pp. 262–279, March 2015.

[13] S. Poirot, S. Bilbao, M. Aramaki, and R. Kronland-Martinet, "Sound morphologies due to non-linear interactions: Towards a perceptive control of environmental sound-synthesis processes," in *Proc. Int. Conf. on*

Dig. Audio Effects, Aveiro, Portugal, Sep. 4–8 2018, pp. 189–196.

[14] T. Taguti, "Dynamics of simple string subject to unilateral constraint: A model analysis of sawari mechanism," *Acoust. Sci. and Tech.*, vol. 29, no. 3, pp. 203–214, 2008.

[15] C. Issanchou, S. Bilbao, J.-L. L. Carrou, C. Touzé, and O. Doaré, "A modal-based approach to the nonlinear vibration of strings against a unilateral obstacle: Simulations and experiments in the pointwise case," *J. Sound Vib.*, vol. 393, pp. 229–251, April 2017.

[16] C. Issanchou, J.-L. Le Carrou, C. Touzé, B. Fabre, and O. Doaré, "String/frets contacts in the electric bass sound: Simulations and experiments," *Appl. Acoust.*, vol. 129, pp. 217–228, 2018.

[17] M. van Walstijn and J. Bridges, "Simulation of distributed contact in string instruments: a modal expansion approach," in *Proc. 24th Euro. Sig. Proc. Conf.*, Budapest, Hungary, Aug. 29–Sept. 2 2016, pp. 1–5.

[18] C. P. Vyasarayani, S. Birkett, and J. McPhee, "Modeling the dynamics of a vibrating string with a finite distributed unilateral constraint: Application to the sitar," *J. Acoust. Soc. Am.*, vol. 125, no. 6, pp. 3673–3682, 2009.

[19] A. K. Mandal and P. Wahi, "Natural frequencies, modeshapes and modal interactions for strings vibrating against an obstacle: Relevance to sitar and veena," *J. Sound Vib.*, vol. 338, pp. 42–59, March 2015.

[20] H. Singh and P. Wahi, "Non-planar vibrations of a string in the presence of a boundary obstacle," *J. Sound Vib.*, vol. 389, pp. 326–349, February 2017.

[21] E. Rank and G. Kubin, "A waveguide model for slap-bass synthesis," in *Proc. IEEE Int. Conf. on Acoust., Speech, and Sig. Proc.*, Munich, Germany, 1997, pp. 443–446.

[22] G. Evangelista and F. Eckerholm, "Player–instrument interaction models for digital waveguide synthesis of guitar: touch and collisions," *IEEE Trans. on Audio, Speech, and Language Proc.*, vol. 18, no. 4, pp. 822–832, 2010.

[23] S. Siddiq, "A physical model of the nonlinear sitar string," *Arch. of Acoust.*, vol. 37, no. 1, pp. 73–79, 2012.

[24] C. P. Vyasarayani, S. Samukham, and S. N. Khaderi, "Nonsmooth modeling of distributed impacts in spatially discretized continuous structures using the ivanov transformation," *arXiv Preprint*, pp. 1–19, 2019. [Online]. Available: arXiv:1908.00486

[25] A. Askenfelt and E. V. Jansson, "From touch to string vibration III: String motion and spectra," *J. Acoust. Soc. Am.*, vol. 93, no. 4, pp. 2181–2196, 1993.

[26] R. C. D. Paiva, J. Pakarinen, and V. Välimäki, "Acoustics and modeling of pickups," *J. Audio Eng. Soc.*, vol. 60, no. 10, pp. 768–782, 2012.

[27] J. Pakarinen and M. Karjalainen, "An apparatus for measuring string vibration using electric field sensing," in *Proc. Stockholm Music Acoust. Conf.*, Stockholm, Sweden, 2003, pp. 739–742.

[28] J. Kotus, P. Szczuko, M. Szczodrak, and A. Czyżewski, "Application of fast cameras to string vibrations recording," in *Proc. 2015 Sig. Proc.: Algorithms, Architectures, Arrangements, and Appl.*, Poznan, Poland, September 2015, pp. 104–109.

[29] Y. Achkire and A. Preumont, "Optical measurement of cable and string vibration," *Shock and Vib.*, vol. 5, no. 3, pp. 171–179, 1998.

[30] M. Podlesak and A. R. Lee, "A photovoltaic detector for string vibration measurement," *J. Acoust. Soc. Am.*, vol. 79, no. 6, pp. 2092–2093, 1986.

[31] D. Kartofelev, M. Mustonen, A. Stulov, and V. Välimäki, "Application of high-speed line scan camera for string vibration measurements," in *Proc. Int. Symp. on Mus. Acoust.*, Le Mans, France, July 2014, pp. 629–634.

[32] M. Mustonen, D. Kartofelev, A. Stulov, and V. Välimäki, "Application of high-speed line scan camera for acoustic measurements of vibrating objects," in *Proc. 7th Forum Acusticum*, Kraków, Poland, September 2014, pp. 1–6.

[33] ——, "Experimental verification of pickup nonlinearity," in *Proc. Int. Symp. on Mus. Acoust.*, Le Mans, France, July 2014, pp. 651–656.

[34] D. Kartofelev, J. G. Arro, and V. Välimäki, "Experimental verification of dispersive wave propagation on guitar strings," in *Proc. 16th Sound and Mus. Comp. Conf.*, Málaga, Spain, May 28–31 2019, pp. 324–331.

[35] D. Kartofelev, A. Stulov, H.-M. Lehtonen, and V. Välimäki, "Modeling a vibrating string terminated against a bridge with arbitrary geometry," in *Proc. 4th Stockholm Music Acoust. Conf.*, Stockholm, Sweden, Jul. 30–Aug. 3 2013, pp. 626–632.

[36] D. Kartofelev, "Kinematics of ideal string vibration against a rigid obstacle," in *Proc. 20th Int. Conf. on Dig. Audio Effects*, Edinburgh, Scotland, UK, September 2017, pp. 40–47.

[37] T. D. Rossing, Ed., *The Science of String Instrumnets*. New York: Springer, 2010.

[38] J. O. Smith, *Physical Audio Signal Processing for Virtual Musical Instruments and Audio Effects*. W3K Publishing, 2010.

[39] D. Kartofelev, A. Stulov, and V. Välimäki, "Pitch glide effect induced by a nonlinear string–barrier interaction," in *Proc. 20th Int. Symp. on Nonlin. Acoust.*, Écully, France, June 29–July 3 2015, p. 030004.